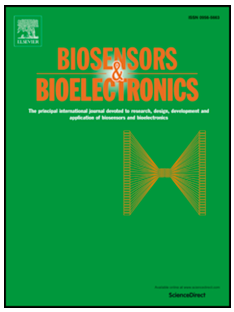

Highly sensitive photoelectrochemical biosensor for microRNA159c detection based on a Ti_3C_2:CdS nanocomposite of breast cancer

Shen-Ting Liu, Xing-Pei Liu, Jing-Shuai Chen, Chang-jie Mao, Bao-Kang Jin

PII: S0956-5663(20)30410-3

DOI: https://doi.org/10.1016/j.bios.2020.112416

Reference: BIOS 112416

To appear in: *Biosensors and Bioelectronics*

Received Date: 21 April 2020

Revised Date: 26 June 2020

Accepted Date: 28 June 2020

Please cite this article as: Liu, S.-T., Liu, X.-P., Chen, J.-S., Mao, C.-j., Jin, B.-K., Highly sensitive photoelectrochemical biosensor for microRNA159c detection based on a Ti_3C_2:CdS nanocomposite of breast cancer, *Biosensors and Bioelectronics* (2020), doi: https://doi.org/10.1016/j.bios.2020.112416.

Shen-Ting Liu: Conceptualization, Investigation, Writing- Original draft preparation **Xing-Pei Liu**: Methodology. **Jing-Shuai Chen**: Validation, Investigation. **Chang-Jie Mao***:* Supervision, Writing- Reviewing and Editing**. Bao-Kang Jin:** Writing- Reviewing and Editing.

Highly sensitive photoelectrochemical biosensor for microRNA159c detection based on a Ti_3C_2:CdS nanocomposite of breast cancer

Shen-Ting Liu, Xing-Pei Liu, Jing-Shuai Chen*, Chang-jie Mao*, Bao-Kang Jin

Key Laboratory of Structure and Functional Regulation of Hybrid Materials (Ministry of Education), Key Laboratory of Chemistry for Inorganic/Organic Hybrid Functionalized Materials of Anhui Province, Key Laboratory of Functional Inorganic Materials of Anhui Province, School of Chemistry & Chemical Engineering, Anhui University, hefei 230601, PR China

Corresponding Author; E-mail: cjshuai@126.com (Chen JS). maochangjie@sina.com (Mao CJ); Tel&Fax: +86 551 6386 1260

ABSTRACT

Herein, an ultra-sensitive photoelectrochemical biosensor based on Ti_3C_2:CdS nanocomposite was established for the selective detection of microRNA159c. Ti_3C_2:CdS nanocomposites were used as optoelectronic materials because Ti_3C_2:CdS interaction effectively separates photogenerated electrons and holes, and significantly improves the high photoelectric conversion efficiency. Firstly, Ti_3C_2:CdS nanocomposite was deposited on the surface of the fluorine-doped tin oxide (FTO) electrode. After the chitosan (CS) was dropped, the SH-miRNA were bonded on the electrode surface via the S-Cd bond. Then 6-mercaptohexanol (MCH) blocked the unbound site, the DNA strand was introduced to hybridize with the target SH-miRNA. At this time, the obtained photocurrent gradually decreases. Subsequently, the photosensitizer TMPyP as signal amplification was modified, the photocurrent increased significantly. The target SH-miRNA was detected based upon the photocurrent change originated from quantities change of TMPyP. Working under the best experimental conditions, the sensing platform had good stability, selectivity, and high sensitivity. The detection range for miRNA159c was 1.0×10^{-6}-1.0×10^{-13} mol·L^{-1}, and the detection limit was approximately 33 fmol·L^{-1}. The detection of miRNA159c

in human serum provided a huge opportunity to explore the relationship between the abundance of this miRNA and the incidence of breast cancer (BC), and to further achieve effective detection of BC.

Keywords: Photoelectrochemical sensor; Ti_3C_2:CdS; miRNA159c; photosensitizer; strand hybridization

1. Introduction

MicroRNA (miRNA) is a type of endogenous noncoding RNA found in eukaryotes that has regulatory functions and is approximately 20-30 nucleotides long (Yi et al., 2019; Bai et al., 2020). Its expression is related to the growth of various human cancer cells (Liu et al., 2019; Li et al., 2020; Wu et al., 2019). For example, miRNA159 is involved in the development of BC. Andrew group found plant miRNA159c in human serum, and its abundance in serum was related to the incidence and progression of breast cancer patients. It also proved for the first time that miRNA159c can affect the growth of BC cells (Chin et al., 2016) and have anti-proliferative capacity against breast cancer cells. Therefore, detection of the miRNA159c can further directly and effectively monitor the patient's condition and realize the effective detection and treatment of tumors in BC patients. Traditional miRNA analysis and detection methods include blot hybridization, microarray, and real-time quantitative polymerase chain reaction. In recent years, a series of analytical methods have been developed, such as the combination of amplification reactions with electrochemistry (Yang et al., 2020; Lu et al., 2020; Wang et al., 2020; Miripour et al., 2020), fluorescence (Zhao et al., 2020; Wang et al., 2020; Li et al., 2020), surface-enhanced Raman scattering (Wang et al., 2019; Si et al., 2020; Cao et al., 2020), and DNA nanotechnology (Shen et al., 2020; Li et al., 2020), which have significantly improved sensitivity. However, these ones existing detection methods require a large number of initial samples during the analysis process or involve a large number of manual operations and complex processing problems, which hinder their further development and application. Photoelectrochemical analysis has the advantages of low background signal, high sensitivity, good specificity, etc., and the

equipment is simple and inexpensive (Devadoss et al., 2015; Zhang et al., 2020). It has become a biological analysis method with great application value in the fields of immunosensing and biomolecule determination. Therefore, this work intends to use photoelectrochemical methods to achieve highly sensitive detection of miRNA159c.

It is well known that improving detection sensitivity is very important for trace samples, especially for complex biological samples. At present, improving sensitivity involves, on the one hand, the development of high photoelectric efficiency materials and, on the other hand, the use of signal transmission or amplification modes. The materials used include CdS, CdSe, CdTe and other quantum dot materials, as well as GO-CdS, MOF-C_3N_4, ZnSe-COOH, TiO_2 nanorods/Au NP composites, etc. However, there are still many deficiencies in the existing photoelectric materials or films in practical applications, such as low photoelectric conversion efficiency, poor stability, and poor repeatability. Some materials meet some requirements to a certain extent, but some require a large number of initial samples during analysis or involve a large number of manual operations and complex processing, which directly limit the further improvement of the performance of photoelectrochemical sensors. These problems directly limit the further improvement of the performance of photoelectrochemical sensors. Therefore, the exploration of new photovoltaic materials is still necessary.

In recent years, new two-dimensional materials—transition metal carbides (MXenes)—have become an emerging research area. As a new transition metal MXenes are widely used in batteries (Xie et al., 2014), electrocatalysis (Wang et al., 2019), thermoacoustic devices (Gou et al., 2019), supercapacitors (Mu et al., 2019; Li et al., 2020), energy conversion (Anasori et al., 2017) and Photodegradation (Huang et al., 2020). Among them, Ti_3C_2 has become a research hotspot because of its excellent performance and has played an important role in many fields. In this work, a method for the composite use of Ti_3C_2 and CdS materials was proposed. The successful implementation of various applications of Ti_3C_2 largely depends on its excellent electronic conductivity, rich exposed metal sites and numerous hydrophilic functions (Liu et al., 2018). Ti_3C_2, as a two-dimensional (2D) layered structure, can effectively improve the efficiency of electron-hole separation because of its higher

electron transport capability (Hemanth et al., 2020; Khazaei et al., 2013; Peng et al., 2016; Zhang et al., 2020). So it is considered one of the most promising light-absorbing materials due to its higher light stability and absorption coefficient. Cadmium sulfide (CdS) has very good photoelectric properties in the visible range (Liu et al., 2018). As the scale decreases, it exhibits different optical and electrical characteristics from its bulk and thin film materials. The quantum size effect of CdS causes the energy level of CdS to change. Due to the trap recombination and complex lattice structure of quantum dots, electron-hole pairs are easily recombined. Therefore, can the combination of Ti_3C_2 and CdS QDs be used as a new optoelectronic material? To answer this question, a sensing platform based on a Ti_3C_2:CdS nanocomposite was established in this work. The band gap of two-dimensional layered Ti_3C_2 could match with energy level of CdS. After CdS QDs excited by an external light source, the photogenerated electrons are quickly transfer from the valence band (VB) to the conduction band (CB). Ti_3C_2 was able to promote the charge transformation and utilization because of its high electron transmission capacity. It is beneficial to transfer the photogenerated electrons to the conduction band of Ti_3C_2 (Yao et al., 2020), and realize the effective separation of photogenerated electrons and holes. Therefore, Ti_3C_2:CdS nanocomposite achieving higher photoelectric conversion efficiency (Scheme 1).

Porphyrins and metalloporphyrins exist widely in nature and in organisms. Each atom is highly conjugated on the same plane, and the complex properties are stable. It can be evenly distributed as a monomer in water and can interact with various biological macromolecules. The porphyrin TMPyP is used as a photosensitizer to achieve signal amplification and obtain an enhanced photocurrent. The working platform can eliminate background signals and effectively improve sensitivity. Based on the excellent characteristics of the sensor, this platform was used for specific detection of microRNA159c.

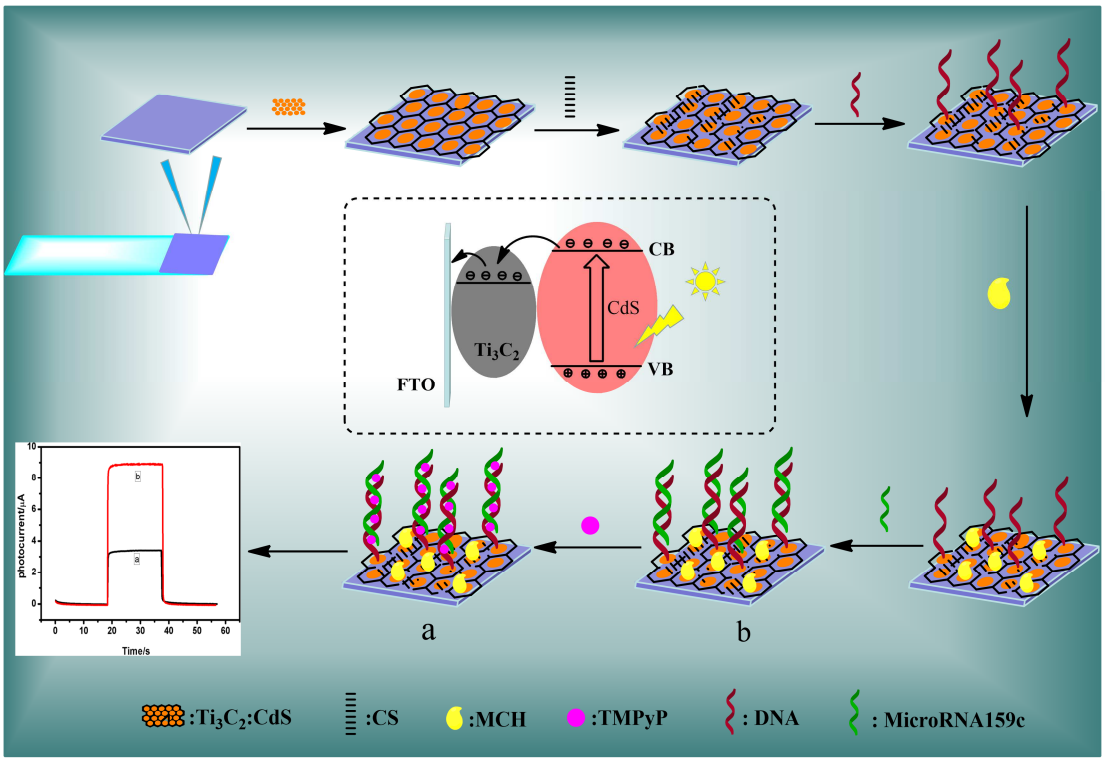

Scheme 1. Schematic diagram of the steps in the construction of a photoelectrochemical biosensor and electronic delivery process.

2. Experimental

Reagents and chemicals, equipment, and some of the solutions used are provided in the supporting materials(Please seen in Supporting Information).

2.1 Synthesis of Ti_3C_2 , CdS QDs and Nanocomposites

The well-formed Ti_3C_2 flakes were prepared according to the literature (Huang et al., 2020), and the preparation process was adjusted. 1.5 g of LiF and 20 ml of 9 M HCl solution were uniformly mixed and reacted briefly, and it was found that LiF was completely dissolved. Then, 0.5 g of Ti_3AlC_2 was added to the reaction system, and the temperature was raised to 35 □ or 24 h.The product was centrifuged at 5,000 r·min^{-1} with secondary water and absolute ethanol, respectively. The product was added with 100 mL of secondary water for 1 h. Centrifugation again, drying at 60 □ to obtain Ti_3C_2.

CdS QDs were prepared according to the literature (Liu et al., 2018). 172μL 3-mercaptopropionic acid was added to 40 ml of 20 mol·L^{-1} $CdCl_2$ solution, adjusted

to pH=11 with NaOH, and passed through N_2 for 30 minutes. 40 mL of 20 mmol·L^{-1} TAA was introduced into the reaction system, and heated to 80□ for 2 hours. Then, cool at room temperature, addabsolute ethanol, let stand overnight, and centrifuge to obtain CdS QDs.

2.2 Synthesis of Ti_3C_2: CdS Nanocomposites

5 mg Ti_3C_2 was dissolved in 5 mL of deionized water and sonicated for 30 minutes. Add 325 μL of CdS QDs, sonicate for 2 hours, through electrostatic bonding.

2.3 Construction of the PEC biosensor platform

The experimental procedure is show in scheme 1. Primarily, FTO conductive glass (Huanan Technology Co., Ltd.) was ultrasonically washed three times with secondary water and C_2H_5OH and dried in an oven overnight. Subsequently, a uniform solution of 30 μL of Ti_3C_2:CdS composite material was uniformly dropped on the surface of the clean bare FTO electrode (0.5 cm × 0.9 cm), dried at room temperature, and allowed to stand for 8 h. The dried electrode was then slowly rinsed with deionized water and blown dry with N_2 to successfully obtain a modified Ti_3C_2:CdS/FTO. Next, 5 μL of CS (1×10^{-6} mol·L^{-1}) was dropped onto the surface of the modified electrode and dried at room temperature for 1 hour. Rinsed slowly with TE buffer solution to remove excess CS on the electrode surface, then blown dry with N_2.. Then, 30 μL of the target miRNA was dropped onto the surface of the electrode and incubated overnight at 4°C. Rinsed slowly with TE buffer solution to remove unbound DNA, then blown dry with N_2. After that, 20 μL of MCH was added dropwise to the electrode slice to block the excess binding sites for 1 h. Rinsed with TE solution to remove excess MCH and blown dry. Then, 30 μL of DNA (2×10^{-6} mol·L^{-1}) was dropped onto the electrode and incubated at 4 □ for 105 minutes to completely hybridize the DNA strand to the RNA strand. Then, 20 μL of TMPyP (20 μmol·L^{-1}) was added dropwise to the electrode surface and incubated for 3 hours. Rinsed and blown dry. Then, the sensor construction was complete (Scheme 1).

2.4 PEC measurement

The electrochemical workstation was equipped with a xenon lamp with a wavelength of 200-1100 nm as a light source, and light-dark current interleaving is

performed every 20 seconds. The test solution was a PBS buffer solution with an AA concentration of 0.1 mol·L^{-1}.

3. Results and discussion

3.1 Characterization of materials

First, TEM was used to explore the morphology of the base material Ti_3C_2 and the nanocomposite Ti_3C_2:CdS. The etched Ti_3C_2 had a better layered structure (Fig. 1A). AFM hatching images indicate that the height of Ti_3C_2 is about 2 nm. (Fig. S1). EDX shows that Ti_3C_2 is composed of two elements, Ti and C, and was successfully prepared (Fig. 1B). Through the combination of positive and negative electricity (Fig. S2), the quantum dots were densely adsorbed on the surface of Ti_3C_2 (Fig. 1C). Clear lattice fringes of CdS QDs were also observed through HR-TEM (Fig. 1D), and the structure is a sphere with an average size of approximately 4.3 nm. The XRD pattern of the sample was recorded (Fig. 1E) (Devadoss et al., 2015; Luo et al., 2016). It also shows that the aluminum layer in titanium aluminum carbon is completely etched, and Ti_3C_2 has been successfully prepared.

To investigate the light absorption of nanomaterials, the UV-visible absorption spectra of the Ti_3C_2:CdS, Ti_3C_2 and CdS were measured (Fig. 1F) (Mostafa et al., 2020; Zhang et al., 2018). After the nanomaterial absorbs ultraviolet and visible radiation, charge transitions occur, and then a band-shaped absorption spectrum is generated. The position of the spectral peak is used to determine the light utilization efficiency of the material. According to the spectrum, Ti_3C_2 has a small amount of absorption in the ultraviolet-visible spectrum wavelength range, while CdS has a strong absorption in the range of 200-400nm. It is obvious that the ultraviolet absorption intensity of the composite material increases and a redshift occurs. This shows that compared with a single material, due to the interaction of Ti_3C_2 and CdS, the composite material has better absorption and higher utilization of light. At the same time, the electron affinity of the composite material increases, the maximum absorption wavelength shifts in the long-wavelength direction, and the energy required for the electron transition decreases. Therefore, Ti_3C_2:CdS has strong optical properties.

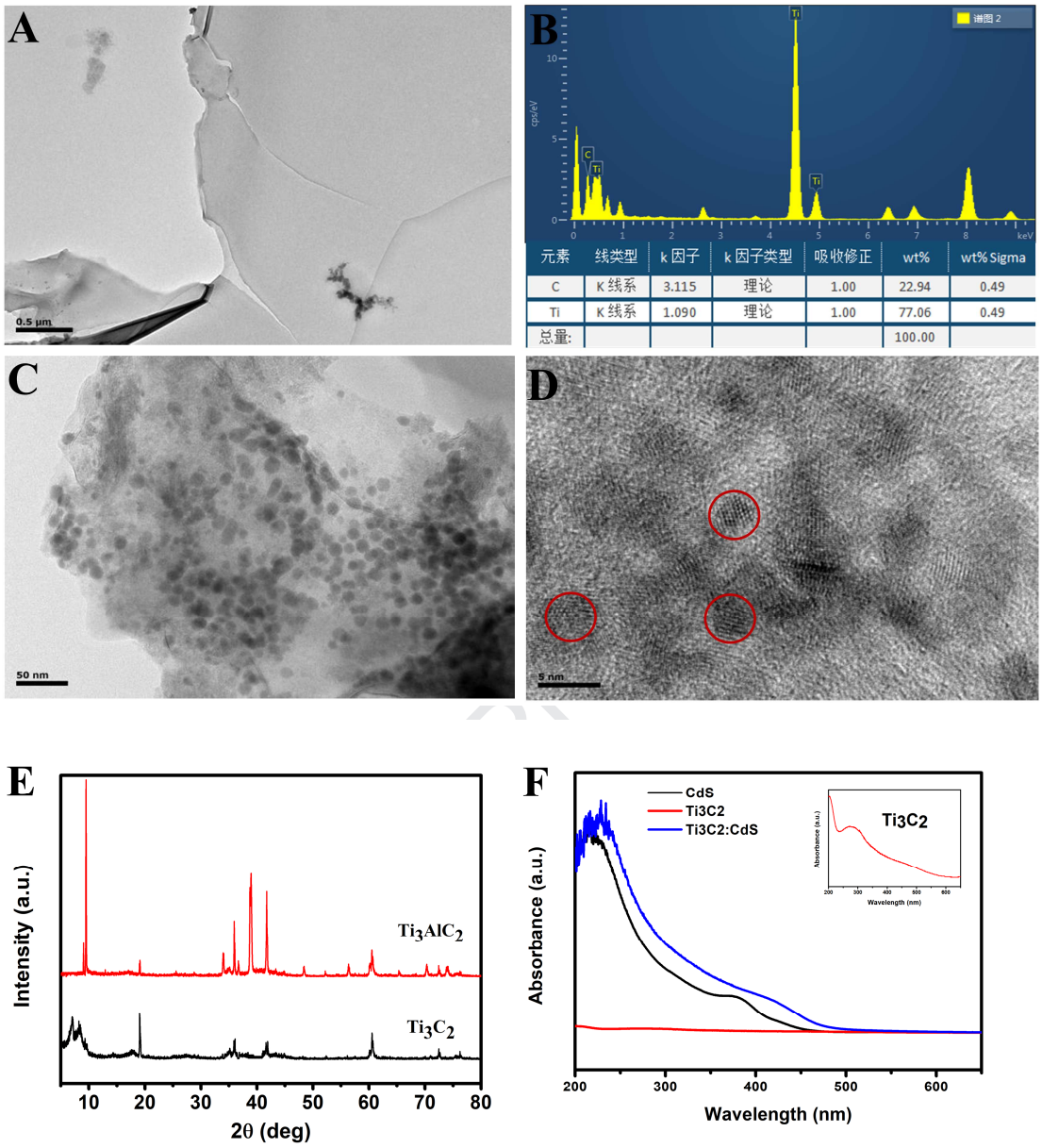

Fig. 1. (A) TEM image of Ti_3C_2, (B) EDX of Ti_3C_2, (C) TEM image of Ti_3C_2:CdS, (D) HR-TEM image of CdS.(E) UV-vis of CdS, Ti_3C_2 and Ti_3C_2:CdS, (F) XRD patterns of Ti_3C_2 and Ti_3AlC_2

X-ray photoelectron spectroscopy (XPS) was used to investigate the molecular structure and chemical bonding of the Ti_3C_2:CdS composites(Fig. 2) (Liu et al., 2018; Li et al., 2019; Braic et al., 2015; Chang et al., 2019; Pazniak et al., 2019). XPS can accurately measure an atom's inner electron binding energy and its chemical shift, providing many types of information for chemical research. The XPS overall spectrum of the complex (Fig. 2A) and the analysis of each element (Fig. 2B) are as follows. In CdS, Cd gives rise to two absorption peaks: Cd $3d_{5/2}$ (405.33 eV) and Cd

$3d_{3/2}$ (411.98 eV) ; Two S peaks also appear: S $2p_{3/2}$ (161.52 eV) and S $2p_{1/2}$ (162.54 eV). Ti 2p has four characteristic absorption peaks: the peak positions are 455.09 eV, 458.72 eV, 461.07 eV, and 464.35 eV, and the corresponding bonds are Ti-C, Ti = O, Ti-C, and Ti = O. C 1s shows four absorption peaks with peak positions at 281.31 eV, 284.75 eV, 286.11 eV, and 288.23 eV. The corresponding chemical bonds are C-Ti, C-H, C-O, and C = O.

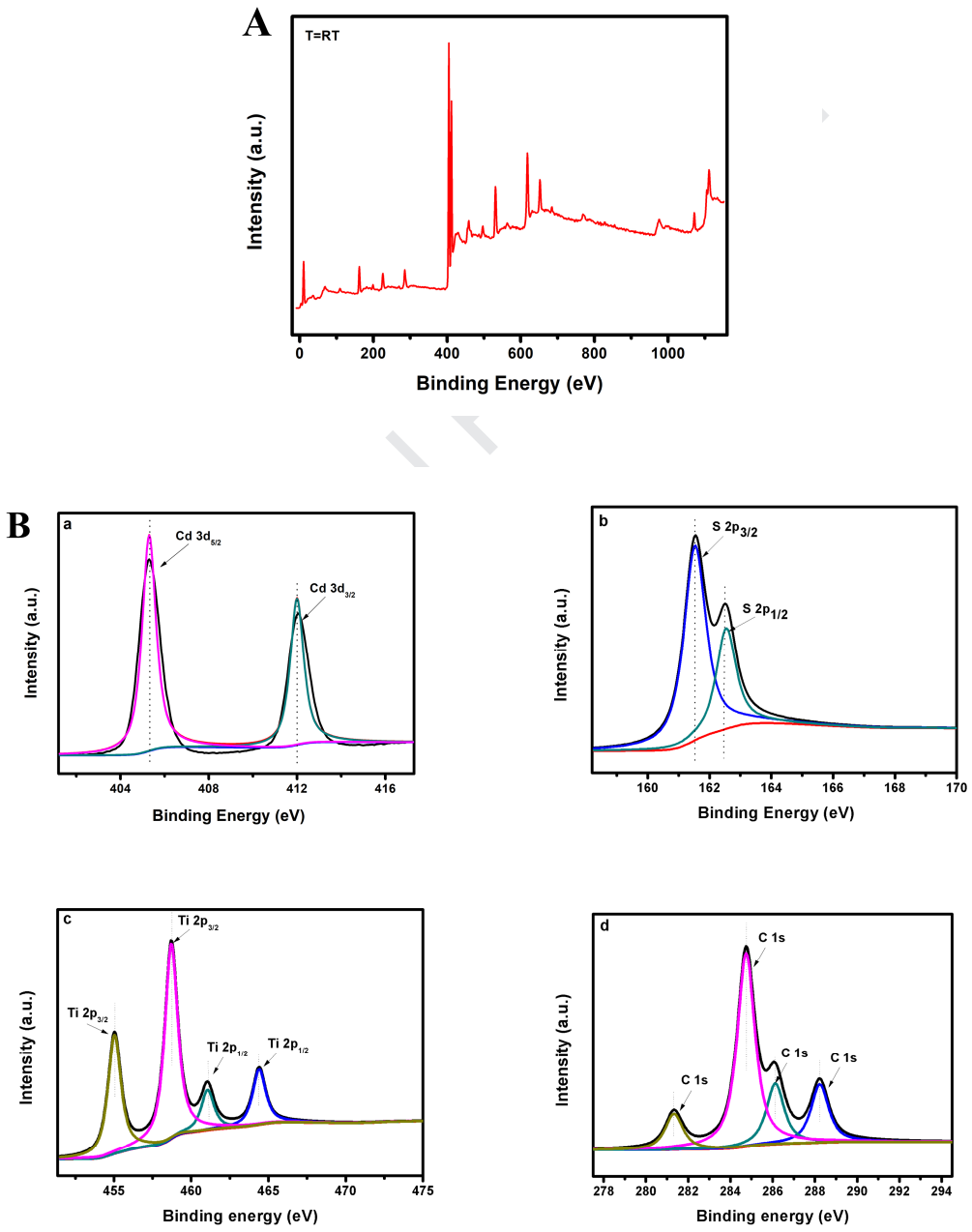

Fig. 2. XPS survey spectra analysis for (A) Ti_3C_2:CdS, (B) plots of (a) Cd, (b) S, (c) Ti and (d) C.

3.2 Photoelectrochemical and EIS behaviors of modified electrodes

We studied the PEC behavior of modified electrodes to varying degrees (Fig. 3A). The PEC response photocurrent of the bare electrode is almost zero. When Ti_3C_2:CdS is modified on the electrode surface, the current reaches a maximum value of 31.2 μA (curve a), indicating that the nanocomposite has good photoelectric properties. When CS, DNA, MCH, and miRNA were sequentially modified onto the electrode surface, the photocurrent decreased gradually (curves b, c, d, e) until it reached a minimum value of 3.4 μA. It may be that the modifier is loaded onto the electrode surface layer by layer, and the substance itself has poor conductivity, resulting in an increase in resistance and a decrease in photocurrent. Finally, after the photosensitizer loading was complete, the photocurrent increased to 11.2 μA due to the sensitization and catalysis of the photosensitizer TMPyP (curve f).

At the same time, to explore the electron conductivity of different modified electrode surfaces, electrochemical alternating current impedance spectroscopy (EIS) was used to characterize the diameter of the high-frequency semicircle equivalent to the resistance of the electrode surface electron transfer process (Fig. 3B). The impedance solution was a 0.01 mol·L^{-1} PBS buffer solution containing 0.2 mM K_3 [Fe (CN) $_6$], K_4 [Fe (CN) $_6$] and 0.01M KCl, pH = 7.4. It can be intuitively seen from Fig. 3A that when the solution resistance and various polarization conditions are ignored, when Ti_3C_2:CdS is modified on the electrode surface, the diameter of the semicircle of the modified electrode becomes larger than that of the bare electrode; that is, the electron transfer resistance (Ret) increases (curve a). The reason for this finding may be the poor conductivity of the modified material. Subsequently, when chitosan (CS), DNA, MCH, and miRNA were sequentially connected to the electrode surface, the impedance value of the entire electrochemical sensor gradually increased (curves b, c, d, e). This indicates that the modifier was successfully loaded onto the electrode surface. The increase in the resistance value may be because the DNA and miRNA strands are long-chain polymers, which have almost no electrical conductivity. Modification of the electrode surface increases the difficulty of electron transfer.

When the photosensitizer TMPyP is loaded onto the electrode surface, the diameter of the semicircle decreases, and the resistance decreases. Most likely due to the sensitization and catalysis of the photosensitizer, the electron transfer ability of the electrode surface is improved, and the impedance value is reduced.

3.3 Optimization of PEC measurement conditions

In this experiment, in order to improve the sensitivity and efficiency of the whole experiment, we have optimized several conditions, including miRNA incubation time, photosensitizer incubation time and concentration. First, whether the incubation time of miRNA is sufficient directly affects whether the DNA and miRNA hybridize completely (Fig. 3C). By optimizing the experiment time, it was found that the photocurrent reached a larger value when the incubation time was 105 minutes. Second, the concentration and incubation time of TMPyP are also key to ensuring full linkage to the hybrid duplex. The optimal concentration was 20 μmol·L^{-1} (Fig. 3D), and the optimal incubation time was 3 hours (Fig. 3E). Under these conditions, the photocurrent is large, and the current is relatively stable. Subsequent experiments were performed using these optimized conditions.

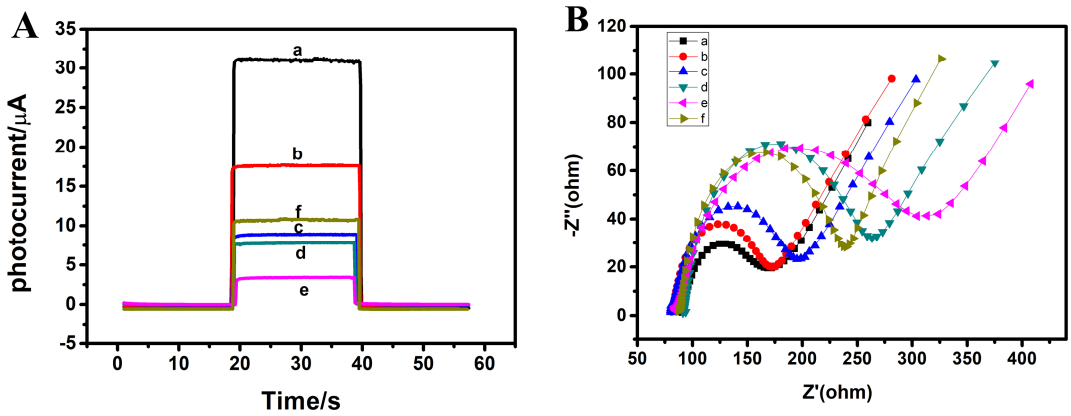

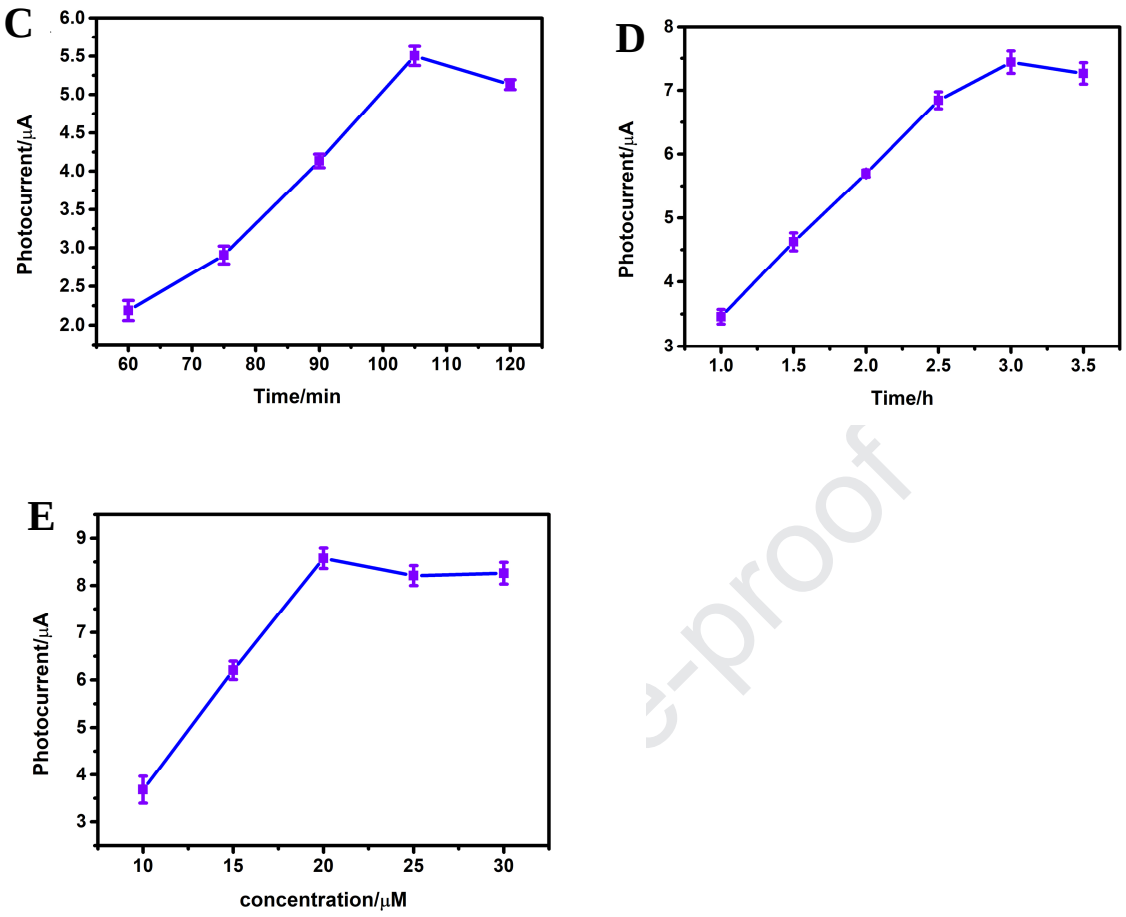

Fig. 3. (A) Photocurrents of the different modified electrodes and (B) EIS responses : (a) Ti_3C_2:CdS/FTO, (b) CS/Ti_3C_2:CdS/FTO, (c) RNA/CS/Ti_3C_2:CdS/FTO, (d)MCH/RNA/CS/Ti_3C_2:CdS, (e)DNA/MCH/RNA/CS/Ti_3C_2:CdS/FTO, (f)TMPyP/DNA/MCH/RNA/CS/Ti_3C_2:CdS/FTO. The effect of (C) the incubation time of miRNA159c, (D) the incubation time and (E) concentration of TMPyP.

3.4 Performance analysis of the developed biosensor

To prove the superiority of the photoelectric properties of the Ti_3C_2:CdS nanocomposite, we performed photocurrent tests on the composite, quantum dots, and pure Ti_3C_2 (Fig. 4A). The corresponding photocurrent response values were 31.03 μA (curve a), 7.93 μA (curve b), and 2.532 μA (curve c). It is clear that the photocurrent of the composite material is much higher than that of a single material and has good photoelectric properties, so the composite was selected as the photovoltaic material

for the experiment.

Under the optimized experimental conditions, the photocurrent response of the designed sensor was enhanced as the miRNA159c concentration increased. The miRNA concentration range was 1.0×10^{-6}-1.0×10^{-13}mol·L^{-1} (Fig. 4B). There was a good linear relationship between the photocurrent and the logarithm of the miRNA159c concentration (Fig. 4C). The linear regression equation is I = 0.9837lgc+17.923, the correlation coefficient is R^2 = 0.9997, and the detection limit is 33 fmol·L^{-1}. Compared with other experimental methods for detecting miRNA (Table S1), the sensor platform in this strategy has a wider linear range and lower detection limit, which shows the excellent performance of the sensor.

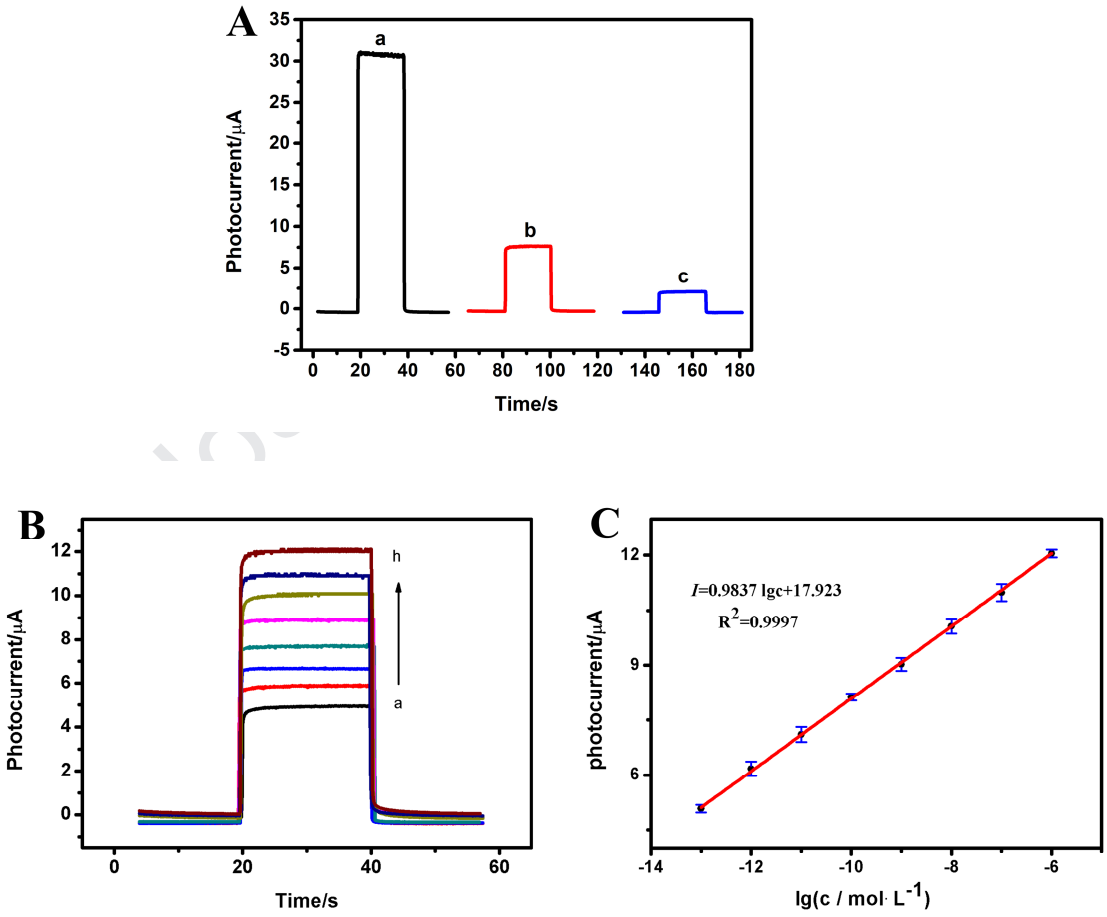

Fig. 4. (A) Photocurrents of the different material: (a) Ti_3C_2:CdS, (b) CdS, (c) Ti_3C_2 , (B) Photocurrent response of different concentrations of miRNA159c and (C) Calibration curve of biosensor platform: (a)10^{-13}mol·L^{-1}, (b)10^{-12}mol·L^{-1}, (c)10^{-11}mol·L^{-1}, (d)10^{-10}mol·L^{-1},

(e)10^{-9}mol·L^{-1}, (f)10^{-8}mol·L^{-1}, (g)10^{-7}mol·L^{-1}, (h)10^{-6}mol·L^{-1}.

3.5 *The stability and selectivity of the constructed PEC biosensor*

To evaluate the selectivity of the designed sensor, some interfering substances were selected and added to human serum samples for detection, including a single-base mismatch target (1MT), a three-base mismatch target (3MT), a noncomplementary sequence (NC), and DENV (Dengue virus) at a concentration of 1.0×10^{-7} mol·L^{-1} instead of miRNA159c with a concentration of 1.0×10^{-8} mol·L^{-1}. The mixed sample contained all interfering RNA in addition to the target (Fig. 5A). It is found that in all interference experiment groups, except for the sample group containing miRNA159c, the PEC response was significantly enhanced after chain hybridization and photosensitizer loading. Therefore, the detection results show that the photoelectrochemical sensor of this strategy has good selectivity for the target miRNA.

In addition, the storage stability of the sensor was tested. The photoelectrochemical sensor of the target miRNA159c was stored in an environment at 4℃ for 33 days. The final test showed that the photocurrent could reach 90% of the original value. At the same time, the photocurrent response for 9 consecutive cycles was recorded with a relative standard deviation of 2.08%（Fig. 5B）. The results show that the sensor has excellent stability and repeatability at room temperature.

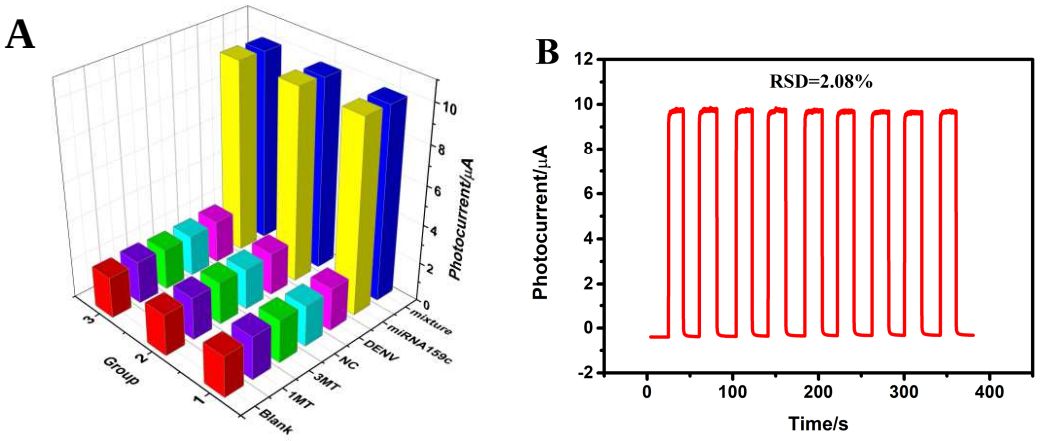

Fig. 5. (A) The responses for different interferences with the 10 times concentration, (B) The stability of the constructed PEC biosensor at 9 cycles (the concentration of miRNA-159c was 1.0×10^{-8} mol·L^{-1}).

3.6 Detection in actual serum samples

The standard addition method was used to explore the application of the sensor in serum samples from BC patients (Table S2). The serum comes from the First Affiliated Hospital of Anhui Medical University. MiRNA159c with different concentration gradients was added to the serum samples. The concentration of added miRNA159c were 0, 10 nmol·L^{-1}, 100 nmol·L^{-1}, 200 nmol·L^{-1}, 300 nmol·L^{-1}. According to the calibration curve (Fig. 4C), the amount of miRNA159c was determined in the serum sample. The calculated recovery range was from 98.89-107.92%, and the relative standard deviation was 1.91-2.43%. Studies have shown that the constructed sensor has high sensitivity and excellent stability, which indicates that the designed PEC sensor has great feasibility in the detection of miRNA and is expected to be applicable to the clinical monitoring of breast cancer.

4. *Conclusion*

In brief, this work uses Ti_3C_2:CdS nanocomposites with excellent photoelectric properties as photoelectric materials. Ti_3C_2 has high electron transport capability, high electrical conductivity, high light stability, and CdS quantum dots (QDs) have unique photoelectrochemical properties. The two are combined as optoelectronic materials. When a light source is added, CdS photogenerated electrons quickly transfer from the valence band to the electron conduction band. When holes are left in the valence band, Ti_3C_2 can help adjust the direction of electron transfer and increase the yield of photogenerated electrons. It effectively reduces the electron-hole reorganization and expands its light-capturing ability. In addition, TMPyP is a photosensitizer that plays a role in signal amplification. The designed biosensor has a relatively wide detection range, low detection limit, good stability and specificity, easy operation and low cost. The range is 1.0×10^{-6}-1.0×10^{-13}mol·L^{-1}, and the detection limit is 33 fmol·L^{-1}. This

novel biosensor for detecting miRNA159c provided a viable option for sensitive detection of other types of microRNAs.

Acknowledgments.

This work was supported by the National Natural Science Foundation of China (Grant Nos. 21575001), Natural Science Foundation of Anhui Province (1508085MB37).

References

Anasori, B., Lukatskaya,M.R., Gogotsi, Y., 2017. Nat. Mater. 16, 34-50.

Bai, Y.Y., Wu, Z., Xu, C.M., Zhang, L., Feng, J., Pang, D.W., Zhang, Z.L., 2020. Anal. Chem. 92, 853-858.

Braic, M., Zoita, N.C., Danila, M. Grigorescu, C.E.A., Logofatu, C., 2015. Thin Solid Films 589,590-596.

Cao, X.W., Wang, Z.Y., Bi, L.Y., Caili Bi, C.L., Qiu Du, Q., 2020. Nanoscale 12, 1513-1527.

Chang, G., Sun, F.Y., Wang, L.H., Che, Z.X., Wang, X.T., Wang, J.G., Kim, M.J., Zhang, H.L., 2019. ACS Appl. Mater. Interfaces 11, 26507-26517.

Chin, A.R., Fong, M.Y., Somlo, G., Wu, J., Swiderski, P., Wu, X.W., Wang, S.E., 2016. Cell Research 26, 217-228.

Devadoss, A., Sudhagar, P., Terashima,C., Nakata, K., Fujishima, A., 2015. J PHOTOCH PHOTOBIO C 24, 43-63.

Gou, G.Y., Ming Liang Jin, M.L., Lee,B., Tian, H., Wu, F., Li, Y.T., Ju, Z.Y., Jian, J.M., Geng, X.S. Ren, J., Wei, Y.H., Jiang, G.Y., Qiao, Y.C., Li, X.S., Kim, S., Gao, M., Jung, H., Won Ahn, C., Yang, Y., Tian-Ling Ren, T.L., 2019. ACS Nano, 13, 12613-12620.

Hemanth, N.R., Kandasubramanian, B., 2020. Chemical Engineering Journal 392, 123678-123692.

Huang, G.M., Li, S.Z., Liu, L.J., Leifan Zhu, L.F., Wang, Q., 2020. APPL SURF SCI 503, 144183-144190.

Khazaei, M., Arai, M., Sasaki, T., Chung, C.Y., Kawazoe Y., 2013. Adv. Funct. Mater. 23, 2185-2192.

Li, C.H., Du, S.W., Wang, H.M., Naghadeh, S.B., Allen, A.L., Lin, X., Li, G.J., Liu, Y., Xu, H., He, C.Q., Zhang, J.Z., Fang, P.F., 2019. CHEM ENG J 378, 122089-122099.

Li, Q., Zhou, S.H., Zhang, T., Zheng, B., Tang, H.W., 2020. Biosens. Bioelectron. 150, 111866-111874.

Li, T., Duan, R.L., Duan, Z.j., Huang, F.j., Xia, F., 2020. Chem. Res. Chinese Universities. 36(2), 194-202.

Liu, X.P., Chen, J.S., Mao,C.J., Niu, H.L., Song, J.M., Jin, B.K., 2018. Anal. Chim. Acta. 1025 ,99-107.

Liu, Y.T., Zhu, X.D., Pan, L., 2018. Small 14, 1803632-1803653.

Liu, Z.M., Wang, Y.M., Li, J.H., Yuan, Y.Y., Wu, X.Y., Liu,W.R., Liu, Y.W., 2019. Anal. Chim. Acta. 1087, 86-92.

Li, Z.Z., Zhang, H.G., Wang, L., Chao, M.X., Shi, J.J., Qi, C.X., Zhang, Z.S., Feng, L.J., Li, C.H., 2020. J Photoch. Photobio. A 386, 112099-112106.

Lu, L.P., Liu, C., Miao, W.J., Wang, X.Y., Guo, G.S., 2020. Anal. Chim. Acta. 1093, 52-60.

Luo, J.M., Tao, X.Y., Zhang, J., Xia, Y., Huang, H., Zhang, L.Y., Gan, Y.P., Liang, C., Zhang, W.K., 2016. ACS Nano 10, 2491–2499.

Miripour, Z.S., Aghaee, P., Abbasvandi, F., Hoseinpour, P., Ghafari, H., Namdar, N., Akbari, M. E., Abdolahad, M., 2020. Biosens. Bioelectron., 161, 112209-112215.

Mostafa, A.M., Mwafy, E.A., Hasanin, M.S., 2020. Opt. Laser Technol. 121,105824-105829.

Mu, X.P., Wang, D.S., Du, F., Chen, G., Wang, C.Z., Wei, Y.J., Gogotsi, Y., Gao, Y., Yohan D, 2019. Adv. Funct. Mater. 29, 1902953-1902958.

Pazniak, A., Bazhin, P., Shplis, N., Kolesnikov, E., Shchetinin,I., Komissarov, A., Polcak, J., Stolin, A., Kuznetsov, D., 2019. Mater. Des. 183, 108143-108149.

Peng, C., Yang, X., Li, Y., Yu, H., Wang, H., Peng, F., 2016. ACS Appl. Mater. Interfaces 8, 6051–6060.

Shen, Z.P., He, L.Y., Wang, W.H., Tan, L., Gan, N., 2020. Biosens. Bioelectron. 148, 111831-111837.

Si, Y.M., Xu, L., Wang, N.N., Zheng, J., Yang, R.H., Li, J.S., 2020. Anal. Chem. 92, 2649-2655.

Wang, D.H., Li, F., Lian, R.Q., Xu, J., Kan, D.X., Yanhui Liu, Y.H., Chen, G., Yury G., Wei, Y.J., 2019. ACS Nano 13, 11078–11086.

Wang, F.F., Fu, C.P., Huang, C., Li, N., Wang, Y.H. Ge, S.G., Yu, J.H., 2020. Biosens. Bioelectron. 150, 111917-111913.

Wang, Z.Y., Xue, J., Bi, C.L., Xin, H., Wang, Y.W., Cao, X.W., 2019. Analyst 144, 7250-7262.

Wang, Z.Z., Xue, Z.Q., Hao, X.L., Miao, C.F., Zhang, J.Z., Zheng, Y.J., Zheng, Z.F., Lin, X.H., Weng, S.H., 2020. Anal. Chim. Acta. 1103 , 212-219.

Wu, T.T., Cao, Y., Yang, Y.M., Zhang, X.Y., Wang, S.T., Xu, L.P., Zhang, X.J., 2019. Nanoscale 11, 11279-11284.

Xie, Y., Agnese, Y.D., Naguib, M., Gogotsi, Y., Barsoum, M.W., Zhuang, H.L., Kent, P.R.C., 2014. ACS NANO 8, 9606-9615.

Yang, J., Xia, Q., Guo, L.H., Luo, F., Dong, Y.Q., Qiu, B., Lin, Z.Y., 2020. Chem. Commun., DOI: 10.1039 / C9CC09706F.

Yao, Z., Sun, H., Sui, H., Liu, X. 2020. Nanomaterials, 10, 452-466.

Yi, W.J., Cai, R.L., Xiang, D.F., Wang, Y.X., Zhang, M.S., Ma, Q.H., Cui, Y.H., Bian**,X.W., 2019. Biosens. Bioelectron. 143, 111614-111619.

Zhang, C., Shuaikai Xu, S.K., Dong Cai, D., Cao, J.M., Wang, L.L., Han, W., 2020, Electrochim. Acta. 330, 135277-135284.

Zhang, H.L., Li, M., Cao, J.L., Tang, Q.J., Kang, P., Zhu, C.X., 2018. Ceram. Int. 44, 19958-19962.

Zhang, K.Y., Lv, S.Z., Zhou , Q., Tang, D.P., 2020. Sens. Actuator B Chem. 307, 127631-127638.

Zhao, H.Y., Wang, M.H., Xiong, X.H., Liu, Y.J. Chen, X.Y., 2020. Talanta 210, 120677-120683.

> A new type of photoelectrochemical sensor was constructed for the detection of MicroRMA 159c.

> MicroRMA 159c was detected for the first time by photoelectrochemical technology.

> The proposed photoelectrochemical protocol presented ultrahigh sensitivity, reproducibility, specificity and stability.

Declaration of interests

☒ The authors declare that they have no known competing financial interests or personal relationships that could have appeared to influence the work reported in this paper.

☐The authors declare the following financial interests/personal relationships which may be considered as potential competing interests: